



Dry reforming of methane with a Ni-based catalyst: a kinetic and thermodynamic analysis

Angel Martinez-Hernandez¹

Received: 3 March 2024 / Accepted: 14 May 2024
© Akadémiai Kiadó, Budapest, Hungary 2024

Abstract

The dry reforming of methane (DRM) was conducted using a Ni-SiO₂ catalysts. It was evaluated the catalyst's stability within the temperature range of 973–1033 K under low spatial time conditions (kinetic regime) in the reactor. The catalyst deactivated more rapidly at high temperatures, contrary to the prediction based on chemical equilibrium calculations. To understand this behavior, it was investigated the impact of reactor operating conditions by simulating the reactor using a pseudo-homogeneous model and comparing the results with the chemical equilibrium prediction. The simulations revealed that, at high spatial times (W/F_{CH_4}), the reactions considered for the DRM process closely approach equilibrium. In contrast, at low spatial times, the reactive system deviates from chemical equilibrium, with the water gas shift and disproportionation of CO being the most favored. This results in increased coke production, which leads to faster catalyst deactivation. The effect is attributed to the kinetic inhibition of CO₂ adsorption, hindering the activation of this molecule at high spatial time. The spatial time in the reactor, whether high or low, strongly depends on the intrinsic catalytic activity of the catalyst. Thus, when studying catalytic solids, the operating conditions of the reactor should be taken into account to avoid erroneous interpretations of the experimental data when evaluating their performance (for example, catalyst selectivity or resistance against deactivation by coke).

Keywords Disproportionation of CO · Deactivation by coke deposition · Effect of reactor operation on the chemical equilibrium · Nickel catalyst deactivation by coke

List of symbols

$K_i(T)$ Theoretical equilibrium coefficient in function of temperature
 T_{Ref} Temperature for the reference (298 K)

✉ Angel Martinez-Hernandez
angel.martinezhn@uanl.edu.mx

¹ Universidad Autónoma de Nuevo León, UANL, Facultad de Ciencias Químicas, Av. Universidad S/N, Ciudad Universitaria, C.P. 66451 San Nicolas de los Garza, Nuevo León, México

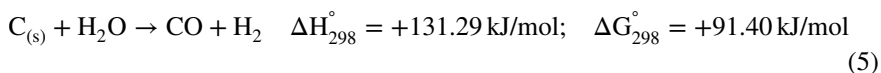
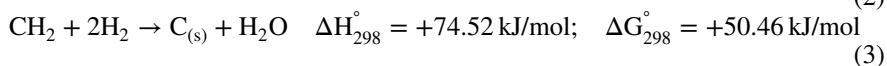
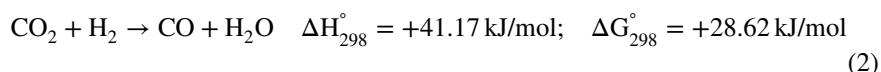
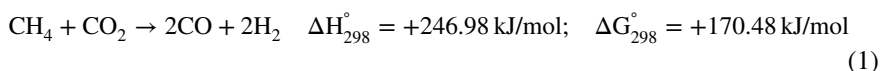
ΔG_{Ref}^o	Free Gibbs energy in standard conditions
ΔH_r	Enthalpy of the chemical reaction
r_i	Reaction rate for the chemical reaction i
k_i	Kinetic coefficient of reaction i
F_i	Molar flow of the compound i
P_T	Total pressure of the reaction system
K_P	Equilibrium coefficient of the reaction rate
$K_{i,j}$	Adsorption coefficient for the compound i in the reaction j
F_T	Total molar flow
L	Reactor Length
D_R	Diameter of the tubular reactor
ρ_{cat}	Density of the catalyst bed
$\frac{dF_i}{dL}$	Differential change of the molar flow of the i compound with reactor length
$\frac{dT}{dL}$	Differential change of the temperature with reactor length
$\frac{dU}{dL}$	Global heat transfer coefficient
T_w	Temperature of the reactor wall
p_j^n	Partial pressure of component j as product
a_j^n	Partial pressure of component j as reactant
n	Stoichiometric coefficient of component j

Introduction

The necessity to mitigate the harmful effects of compounds produced in anthropogenic processes that play an important role in the greenhouse effect has become a major concern for the scientific community. This has prompted research to find techniques capable of decreasing their impact on the environment. Among such compounds, methane and carbon dioxide (both with a high greenhouse potential) are of particular interest because both are produced from organic decomposition (for example, from organic waste in urban settings) and can be used almost directly (with prior treatment, e.g., removal of sulfur compounds) to produce the so-called syngas (H_2 and CO) in a catalytic reactor. The syngas could then be used in different ways, either by separating the H_2 for to be used in power cells, to produce synthetic oil (Fischer–Tropsch reaction) or valuable chemicals (such as alcohols, for instance) [1, 2].

The reaction between methane and carbon dioxide is known as dry reforming of methane (DRM) and has been widely studied using different reaction systems to overcome the thermodynamically limited reactions. For example, thermo-catalysis, thermo-photo coupled catalysis, as well as non-thermal plasma (NTP) and plasma-assisted catalytic DRM [3, 4]. However, the main drawback for the commercial use of this process is that there are side reactions that promote the production of carbonaceous deposits (coke), in addition to the high amount of energy required to perform the endothermic reaction [1].

Significant efforts have been made to minimize coke production, for example, by fine-tuning the formulation of the catalysts [2, 5–8]. Complications arise because, in addition to the dry reforming of methane (DRM) reaction (Eq. 1), there are parallel reactions that lead to the undesirable production of coke. Iyer et al. [9] conducted a kinetic study of the DRM process and proposed that the reaction results could be adequately represented by considering the reverse of the water gas shift reaction (RWGS) (Eq. 2), methane decomposition (Eq. 3), and the reverse of the Boudouard reaction (Eq. 4) together with the DRM reaction (Eq. 1). Reactions (Eqs. 3 and 4), in their reverse form, are essentially the reason why this process is quite difficult to perform under practical conditions, due to their high potential for coke production, usually in the form of filaments that block catalyst pores and voids. This can eventually force the shutdown of the process by obstructing the flow through the reactor [10–12].



On the other hand, it has been reported that depending on the composition of the reaction mixture, coke could either be produced or gasified during the DRM process (Eqs. 3–5) [13]. Therefore, an analysis that includes the chemical equilibrium and the kinetic rates of the main reactions can be very useful for explaining the differences in the observed behavior during the evaluation of catalytic solids for the DRM reaction. For example, Ginsburg et al. [14] conducted a study of the DRM using a CREC riser simulator, and found from a thermodynamic and kinetic analysis that there is a correlation between coke production and the occurrence of the carbon monoxide disproportionation reaction in the reactor. Moreover, Benguerba et al. [15] and Zambrano et al. [13] suggested that the experimental data obtained during the dry reforming of methane (DRM) process can be effectively described using the reactions presented in Eqs. 1–5. Although they differ in their consideration of the initial direction of reactions (Eqs. 4 and 5), both studies essentially describe the same reaction system. However, despite the complete equivalence of the reaction systems, there could be a significant difference in the understanding of the reaction pathway. This disparity may impact the proposed models and their ability to accurately describe the overall reaction and its sub-reactions in the context of dry reforming of methane (DRM). In this context, the activation of CH_4 and CO_2 on the catalyst surface to produce H_2 and CO during the DRM reaction has been extensively studied in the literature, both theoretically and experimentally. These serve

as the basis for the reaction rate equations with mechanistic fundamentals found in existing literature [10]. In the specific context of Ni-based catalysts, recent efforts to describe the dry reforming of methane (DRM) process involve studies that utilize thermodynamic calculations and propose micro-kinetic models, taking into account adsorbed species and reaction intermediates. For instance, Delgado et al. [16] conducted a comprehensive study, applying both approximations to the reforming of CH_4 with CO_2 and H_2O , as well as partial oxidation with O_2 . They observed a reasonably good agreement between thermodynamic predictions and micro-kinetic modeling, aligning with their experimental results. Based on their theoretical work, they concluded that CH_4 activation is the most sensitive reaction in DRM. Specifically, they proposed that adsorbed CH_4 ($\text{CH}_4(\text{s})$) can react either with a Ni site or an adsorbed oxygen atom (O) to form $\text{CH}_3(\text{s})$ and $\text{H}(\text{s})$ or $\text{OH}(\text{s})$, both exhibiting nearly identical sensitivity coefficients. More recently, Rakhi et al. [17] introduced a variation of the reaction set proposed by Delgado et al. In their study, they found that the reaction of $\text{CH}_4(\text{s})$ with a Ni site to produce $\text{CH}_3(\text{s})$ and $\text{H}(\text{s})$ was three times more sensitive than the reaction leading to $\text{OH}(\text{s})$. Although these two studies have demonstrated that their models for the dry reforming of methane (DRM) reaction can reasonably describe experimental results, significant discrepancies and uncertainties persist regarding the existence of the proposed species. These limitations hinder their predictive capability, especially concerning the formation of solid carbon. Therefore, understanding the dry reforming of methane (DRM) process is crucial for practical implementation, as the control of these sensitive reactions could enable the manipulation of the reaction pathway and prevent undesirable routes, such as the production of solid carbon. Additionally, the challenge lies in considering reactor operation effects. Comparing thermodynamic predictions with experimental data necessitates obtaining data from the reactor outlet under chemical equilibrium conditions, which is not always feasible due to operational conditions in the reactor.

The aim of this work is to rationalize the deactivation caused by the formation of solid carbon (coke) during the DRM reaction over a Ni-based catalyst with the reactor operating under kinetic conditions and to identify the effect of the reactor operation conditions on the catalyst deactivation. Understanding these effects could be useful to avoid misinterpretations of the experimental results, such as catalyst selectivity or resistance against deactivation. This is particularly important in cases where the effect of the operating conditions of the reactor is not taken into account.

Chemical equilibrium and simulation of the reactor

Chemical equilibrium

No water vapor was observed in the reactor effluent in any of the experiments; thus, it was considered that this compound is consumed by the reaction with CH_4 and carbonaceous deposits (coke). The calculation of chemical equilibrium was performed using the reactions shown in Eqs. 1–5, with the addition of the steam methane reforming ($\text{CH}_4 + \text{H}_2\text{O} \rightarrow \text{CO} + 3\text{H}_2$). The chemical equilibrium prediction was compared using two methods: (i) the first method (M1) involved calculating the

equilibrium coefficient for all reactions at 298 K, which served as the reference temperature (according to Eq. 6). Then, using the Van't Hoff equation, the equilibrium coefficient at a higher temperature was calculated (Eq. 7). Once the equilibrium coefficient at a higher temperature for all the considered reactions was calculated, the reaction mixture composition was determined by simultaneously solving the resulting equations from Eq. 8 for the six reactions. The algorithm for the calculation of the chemical equilibrium was implemented in Scilab [18], using a tolerance of 1.5×10^{-7} as the convergence criteria; (ii) For the second method (M2), the software DWSIM [19] was employed to model the six reactions within a Gibbs reactor, with the goal of minimizing Gibbs energy. In both methods, ideal gas behavior was assumed, and therefore, Raoult's law was utilized for the calculations. Considering that the intention is to compare simulation predictions with experimental data obtained at $P=1$ atm, the consideration of ideality can work reasonably well and facilitate the calculations.

$$K_i(T_{Ref}) = \exp\left(\frac{-\Delta G_{Ref}^o}{RT_{ref}}\right) \quad (6)$$

$$\ln\left(\frac{K(T)}{K(T_{Ref})}\right) = -\frac{1}{R} \int_{T_1}^{T_2} \frac{\Delta H_r}{T^2} dT \quad (7)$$

$$K_i(T) = \frac{\prod_1^j p_j^n}{\prod_1^j a_j^n} \quad (8)$$

Simulation of the reactor

Since the H_2O compound produced from the reaction shown in Eq. 2 was not observed in our experimentation (similar to many reports in the available literature), it was supposed that its amount in the reactive mixture is very small and therefore not kinetically relevant to promote the steam methane reforming. Therefore, this reaction was not included in the reactor modeling. Cherbański et al. [20] used the set of reactions proposed by Benguerba et al. [15], finding that these five reactions (Eqs. 1–5) reasonably described their experimental data for a Ni-based catalyst. Thus, in this work, the set of reactions and the kinetic rates proposed by Benguerba et al. were used for the simulation of the reactor. The equations were adapted as shown in Eqs. 9–13, and the values for the kinetic and adsorption coefficients were the same as those reported therein. The reason for using the same parameters reported by Benguerba et al. was to examine general trends in the reactor performance using the reactor simulation and contrast these with the experimental results. This would allow the identification of the effects promoted by the operating conditions of the reactor, regardless of the intrinsic activity of the Ni-based catalyst (laboratory-studied catalysts usually have higher activity

than industrial ones). In this work, it is assumed that the effect of the kinetic parameters (intrinsic activity of the catalyst) could shift the obtained curves along the reactor length, but the general trend in the reactor is maintained.

For the kinetic analysis, a pseudo-homogeneous reaction system was considered for modeling the reactor (Eqs. 14–18). The sensible heat for the reaction mixture was calculated considering the following six compounds: CH₄, CO₂, CO, H₂, H₂O, and He, whereas the reaction heat was calculated considering the five reactions shown in Eqs. 1–5. The pressure drop in the reactor was neglected, and the energy balance for the reactor is shown in Eq. 19. The algorithm for solving the system of differential equations (Eq. 14–19) was implemented in Spyder (Python) [21]. The parameters used for the simulation of the reactor are shown in Table 1.

$$r_1 = \frac{k_1 K_{CO_2'} K_{CH_4'} F_{CH_4} F_{CO_2} P_T^2}{\left(F_T + K_{CO_2'} F_{CO_2} P_T + K_{CH_4'} F_{CH_4} P_T\right)^2} \left[1 - \frac{(F_{CO} F_{H_2})^2 P_T^2}{K_{P_1} F_{CH_4} F_{CO_2} F_T^2}\right] \tag{9}$$

$$r_2 = \frac{k_2 K_{CO_2'} K_{H_2'} F_{CO_2} F_{H_2} P_T^2}{\left(F_T + K_{CO_2'} F_{CO_2} P_T + K_{H_2'} F_{H_2} P_T\right)^2} \left[1 - \frac{F_{CO} F_{H_2 O}}{K_{P_2} F_{CO_2} F_{H_2}}\right] \tag{10}$$

$$r_3 = \frac{\left(k_3 K_{CH_4'} F_T P_T\right) \left[F_{CH_4} - \frac{(F_{H_2}^2 P_T)}{K_{P_3} F_T}\right]}{\left[F_T + K_{CH_4'} F_{CH_4} P_T + \left(\frac{1}{K_{H_2'} F_T^{0.5}}\right) F_{H_2}^{1.5} P_T^{0.5}\right]^2} \tag{11}$$

Table 1 Parameter values used for the reactor simulation with $R = CO_2/CH_4 = 1$

Pressure (Bar)	1
Total inlet flow (cm ³ /min)	70
Reactor length (cm)	320
Reactor diameter (cm)	1
Global heat transfer coefficient (J/s cm ² K)	0.037
Molar flow of He (mole/min)	8.03 × 10 ⁻⁴
Molar flow of CO ₂ (mole/min)	8.03 × 10 ⁻⁴
Molar flow of CH ₄ (mole/min)	8.03 × 10 ⁻⁴
Catalyst density (kg/cm ³)	4.5 × 10 ⁻⁴

$$r_4 = \frac{\left(\frac{k_4}{K_{H_2O}'}\right) \left[\left(\frac{F_{H_2O}}{F_{H_2}}\right) - \left(\frac{F_{CO}P_T}{K_{P_4}F_T}\right) \right]}{\left[1 + \frac{K_{CH_4}'P_T}{F_T} F_{CH_4} + \frac{F_{H_2O}}{K_{H_2O}'F_{H_2}} + \left(\frac{1}{K_{H_2}'}\right) \left(\frac{F_{H_2}}{F_T}\right)^{1.5} \right]^2} \quad (12)$$

$$r_5 = \frac{\left(\frac{k_5}{K_{CO}'K_{CO_2}'}\right) \left[\left(\frac{F_{CO_2}}{F_{CO}}\right) - \left(\frac{F_{CO}P_T}{K_{P_5}F_T}\right) \right]}{\left[1 + K_{CO}'\left(\frac{F_{CO}}{F_T}\right)P_T + \left(\frac{1}{K_{CO}'K_{CO_2}'}\right) \left(\frac{F_{CO_2}}{F_{CO}}\right) \right]^2} \quad (13)$$

Material balance

$$\frac{dF_{CH_4}}{dL} = \frac{\pi \rho_{cat} D_R^2}{4} (r_1 + r_3) \quad (14)$$

$$\frac{dF_{CO_2}}{dL} = \frac{\pi \rho_{cat} D_R^2}{4} (r_1 + r_2 + r_5) \quad (15)$$

$$\frac{dF_{CO}}{dL} = \frac{\pi \rho_{cat} D_R^2}{4} (2r_1 + r_2 + r_4 + 2r_5) \quad (16)$$

$$\frac{dF_{H_2}}{dL} = \frac{\pi \rho_{cat} D_R^2}{4} (2r_1 - r_2 + 2r_3 + r_4) \quad (17)$$

$$\frac{dF_{H_2O}}{dL} = \frac{\pi \rho_{cat} D_R^2}{4} (r_2 - r_4) \quad (18)$$

Energy Balance

$$\frac{dT}{dL} = \frac{\left[\pi D_R U_w (T_w - T) + \left(0.25 \rho_{cat} \pi D_R^2 \sum_{i=1}^5 r_i \Delta H_r \right) \right]}{F_T \sum_{i=1}^6 F_i C_{p_i}} \quad (19)$$

Experimentation

Catalyst synthesis

Two types of catalysts were used in this study: one with the Ni incorporated since the synthesis of the support (Ni-m10) and the other by incipient impregnation (Ni-i10), where 10 indicates the weight percentage of Ni in the catalysts. The synthesis

of the SiO₂ support was reported previously [22]. Briefly, it was prepared using a mixture of tetraethyl orthosilicate (SiO₄(C₂H₅)₄, Sigma-Aldrich), ethanol, and dodecylamine (CH₃(CH₂)₁₅NH₂, Sigma Aldrich). The Ni-m10 catalyst was prepared by mixing a certain amount of Ni(NO₃)₂ (Sigma Aldrich) with 20 ml of ethylene glycol (Sigma Aldrich); the mixture was aged and then added to the tetraethyl orthosilicate (TEOS) to obtain "Ni-modified TEOS," which was separated and mixed with dodecylamine and an ethanol/water solution. The Ni-i10 catalyst was prepared as a contrast by the incipient wetness method, using the SiO₂-synthesized support and a solution of the Ni nitrate salt. The SiO₂ support, Ni-m10, and Ni-i10 catalysts were calcined at 823 K in static air for 6 h to remove the organic template.

Catalytic activity

The DRM reaction was carried out in a tubular quartz micro-reactor ($\phi = 11$ mm). The reactor feed consisted of an equimolar amount of CH₄ (50% in He, INFRA) and CO₂ (industrial grade, INFRA) with He balance. The total flow through the reactor was 70 cm³/min. For the high and low spatial times, the mass of catalyst loaded in the reactor was 20 mg ($W/F_{\text{CH}_4} = 7.84 \times 10^{-6}$ g_{cat} min cm⁻³) and 1 mg ($W/F_{\text{CH}_4} = 3.92 \times 10^{-7}$ g_{cat} min cm⁻³), using the SiO₂ support as a diluent in order to keep the bed thickness constant in the reactor. The catalysts were reduced in-situ at 973 K using a mixture of 5% H₂ in N₂ balance prior to the catalytic tests. The reactants and the reactor effluent were analyzed online using a gas chromatograph (Shimadzu, GC-15A) equipped with a thermal conductivity detector and a Porapak-N packed column.

Results and discussion

In Fig. 1, the results obtained from the chemical equilibrium calculation for an equimolar reaction mixture ($R = 1$) are depicted. It can be observed that below 773 K, the calculations using method M1 predict a substantial extent of reaction between CH₄ and CO₂, leading to the formation of H₂O and coke (see Fig. 5). The production of H₂O reaches a maximum at 505 K, after which it decreases with the increase in temperature. Above 900 K, the molar fractions of H₂O and CO₂ are almost equal and follow the same decreasing trend. In Fig. 1, important discrepancies are observed in the predictions made by the M1 and M2 methods, particularly at low temperatures. While the M1 method predicts a substantial amount of water and significant conversion of CH₄ and CO₂ at low temperatures ($T \leq 500$ K), the M2 method predicts that the reaction will commence at $T > 500$ K. Table 2 displays the equilibrium coefficients calculated using both methods. Notably, with the M1 method, reaction (Eq. 3) ($\text{CH}_4 \rightarrow \text{C}_{(s)} + \text{H}_2$) and reaction (Eq. 2) ($\text{CO}_2 + \text{H}_2 \rightarrow \text{CO} + \text{H}_2\text{O}$) are overpredicted; there is a difference of six orders of magnitude at 298 K between the two methods for reaction (Eq. 3). These differences explain why the M1 method predicts a large amount of H₂O at low temperature. The inflection in the CH₄ curve around 600 K occurs because

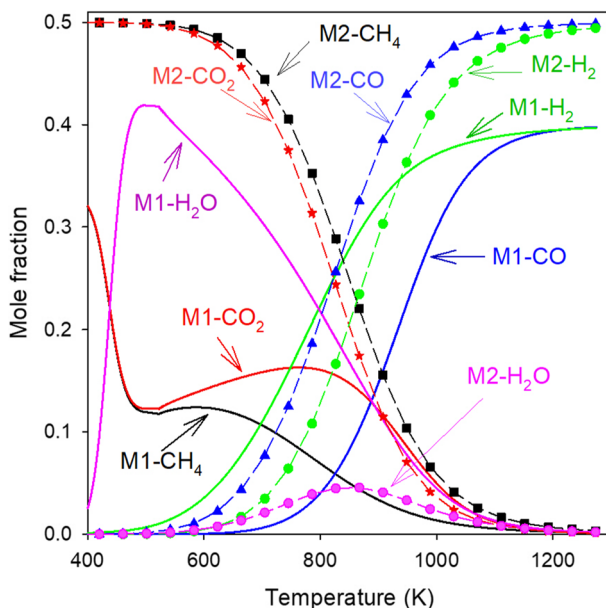


Fig. 1 Composition of the reaction mixture (excluding solid carbon production) at chemical equilibrium. The equilibrium was calculated using both the M1 and M2 methods for an equimolar reaction feed ($R = \text{CO}_2/\text{CH}_4 = 1$)

Table 2 Comparison of equilibrium coefficients (K) calculated with Raoult's law at 1 atm

T (K)	Gibbs energy minimization obtained with DWSIM software [19]			Calculated with the procedure described in "Chemical equilibrium" section		
	Rxn 1	Rxn 2	Rxn 3	Rxn 1	Rxn 2	Rxn 3
298	1.38×10^{-30}	9.86×10^{-6}	6.50×10^{-15}	1.35×10^{-30}	9.68×10^{-6}	1.44×10^{-9}
663	2.56×10^{-6}	0.07	6.17×10^{-4}	2.64×10^{-6}	0.08	5.27×10^{-2}
1029	45.02	0.78	4.73	46.29	0.82	14.04
1273	14,966.34	1.65	74.91	15,447.69	1.73	106.11
T (K)	Rxn 4	Rxn 5	SMR	Rxn 4	Rxn 5	SMR
298	2.13×10^{-16}	2.16×10^{-11}	1.40×10^{-25}	9.37×10^{-22}	9.68×10^{-17}	1.40×10^{-25}
663	4.16×10^{-3}	5.57×10^{-2}	3.44×10^{-5}	5.01×10^{-5}	6.55×10^{-4}	3.45×10^{-5}
1029	9.51	12.12	57.40	3.30	4.02	56.42
1273	199.80	120.89	9055.53	145.58	83.97	8910.88

Rxn 1 to 5 refers to reactions shown in Eqs. 1–5, while SMR refers to steam methane reforming reaction

reaction (Eq. 1) ($\text{CH}_4 + \text{CO}_2 \rightarrow 2\text{CO} + 2\text{H}_2$) begins to be favored and competes with reaction (Eq. 3). Similarly, in the CO_2 curve, the inflection occurs around 800 K due to the promotion of CO_2 consumption by reaction (Eq. 2) through the H_2 produced in reaction (Eq. 3), which hinders reaction (Eq. 1). A different

scenario is observed with the M2 method, which predicts that there is no significant CH_4 and CO_2 consumption below 600 K. Additionally, a lower H_2O production is predicted because reaction (Eq. 3) is less favored with this method. The predictions from the M2 method align more closely with experimental results for gaseous compounds (see Figs. 3, 4 and S2). However, it was not possible to estimate the amount of solid carbon production using this method. In contrast, the M1 method allowed for such estimation. Consequently, the calculations of solid carbon production obtained with the M1 method will be used to rationalize the reactor simulation and experimental results for the deactivation of Ni-m10 and Ni-i10 catalysts.

The results for the reactor simulation at 973 K with an equimolar reaction mixture ($R=1$) are shown in Fig. 2. It can be seen that the highest reaction extent occurs at the entrance of the reactor (approximately the first 60 cm), and from $L=200$ cm, the molar flows show a nearly constant value (this simulation was used as a reference to set the reactor length at 320 cm for all simulations). Furthermore, the most significant temperature drop occurs at the reactor entrance due to endothermic reactions (as depicted in Fig. S1). However, due to the low amount of reactants, there is only a minimal change in temperature (approximately 1.6 K). In practical terms, the reactor operates under isothermal conditions. The quantities of CO_2 and H_2O at the reactor outlet are similar, consistent with the predictions of chemical equilibrium calculated using the M2 method, which suggests a slightly lower amount of H_2O . Despite both the chemical equilibrium and reactor simulation predicting the production of H_2O and its presence in the reactor outlet, this was not detected in any of our

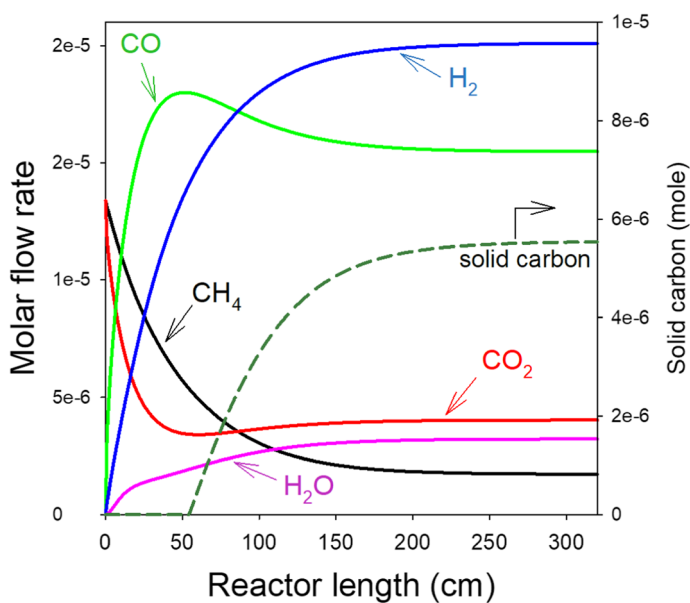


Fig. 2 Composition of the reaction mixture along the reactor length obtained from the reactor simulation at 973 K. $W/F_{\text{CH}_4} = 23.632 \text{ g}_{\text{cat}} \text{ min cm}^{-3}$

experiments. Apart from the possible consumption of H_2O by reaction with the CH_4 and coke mentioned above, their reaction with the active metal sites on the catalyst can severely affect the experimental results, leading to a loss in catalytic activity. Furthermore, the reaction atmosphere could promote the migration of the metal sites, resulting in the sintering of the metal particles, which also causes catalyst deactivation [11, 23]. All these phenomena could introduce bias into the information extracted from the experimental results, making it important to carefully consider and account for these aspects in the catalytic tests. On the other hand, Fig. 2 reveals that the amount of coke increases in proportion to the reactor length. This phenomenon arises from consecutive coking reactions [24], while the curve trend obtained in the simulation aligns with the results reported by Delgado et al. [16] that calculated the surface coverage of carbon along the catalytic bed in a tubular fixed bed reactor.

Subsequently, the values predicted in the reactor simulation at the outlet and the chemical equilibrium calculations will be used to rationalize the obtained experimental results for the synthesized Ni catalysts. Fig. 3 compares the conversions of CH_4 (Fig. 3a) and CO_2 (Fig. 3b) calculated with the chemical equilibrium, the reactor simulation, and the experimental data obtained with the Ni-i10 and Ni-m10 catalysts, with the reactor operating under higher spatial time conditions ($W/F_{\text{CH}_4} = 7.84 \times 10^{-6} \text{ g}_{\text{cat}} \text{ min cm}^{-3}$). Below 973 K, the CH_4 and CO_2 conversions predicted by the M1 method in chemical equilibrium are higher than those obtained in the reactor simulation and experimental tests. In contrast, the results from the M2 method are closer to both. However, at high temperatures ($T > 973 \text{ K}$), the M2 method aligns more closely with the reactor simulation results for CH_4 conversion, while the opposite occurs for CO_2 conversion, where the M1 method prediction overlaps the reactor simulation curve. The conversions of CH_4 and CO_2 for the Ni-m10 catalyst were lower than those obtained with Ni-i10, indicating that the reaction rate is slow in the case of the former catalyst. Moreover, the experimental CO_2 conversion for both catalysts exceeded the predictions made using the M1 method and reactor simulation, but the M2 method closely described the results for the Ni-i10 catalyst. It is usually expected that the conversion predicted by chemical equilibrium will be higher than that obtained experimentally or even through simulations using kinetics data, especially at low temperatures. This occurs because the catalytic sites are not active under such temperature conditions. These differences can explain the observed variations in CH_4 and CO_2 conversions, as well as the H_2/CO ratio (as shown in Fig. 4) obtained with the Ni-i10 catalyst when compared to the chemical equilibrium predicted using the M1 method. Nevertheless, the proximity of the experimental data for CH_4 and CO_2 conversions to the reactor simulation curve between 673 and 1173 K suggests that the reaction scheme proposed in Eqs. 1–5 could serve as a useful representation for the DRM reaction.

On the other hand, below 900 K, the experimental H_2 yield closely matches the prediction from the reactor simulation. Above this temperature, the experimental data also align with the equilibrium curve predicted by both methods. Regarding CO yield, below 973 K, the values from the equilibrium curve predicted using the M1 method are lower than the experimental data (which align with the reactor simulation). In contrast, the M2 method predicts greater production across the entire temperature range. Above 1073 K, both the reactor simulation and the M1 and M2

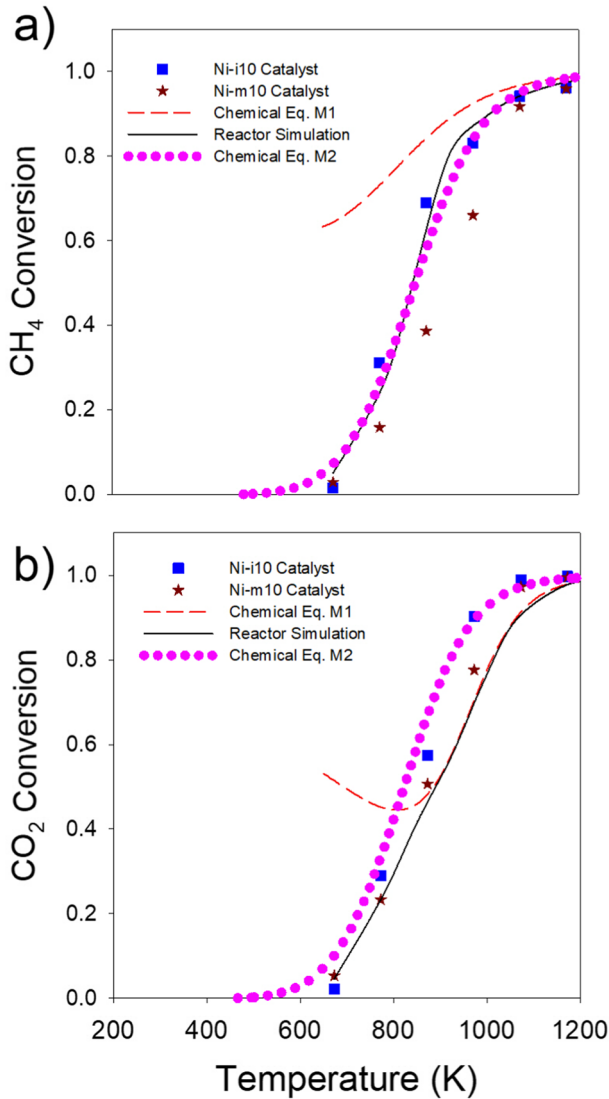


Fig. 3 Conversion of CH_4 (a) and CO_2 (b) versus temperature. Experimental data (black star Ni-m10, black square Ni-i10), Chemical equilibrium calculations (M1 method: dashed line, M2 method: dotted), and reactor simulation (solid line) with an equimolar reaction mixture ($R = \text{CO}_2/\text{CH}_4 = 1$). The experimental data were obtained with $W/F_{\text{CH}_4} = 7.84 \times 10^{-6} \text{ g}_{\text{cat}} \text{ min cm}^{-3}$

chemical equilibrium methods predict a high CO yield; nevertheless, the experimental data fall below the simulated curves (Fig. S2). This suggests that at high temperatures ($T > 1000 \text{ K}$), the reaction of CO disproportionation is favored in both catalysts during the DRM reaction [7]. Fig. 4 shows the H_2/CO ratio, where it can be seen that kinetically, the relevant temperature for the DRM reaction is above 900 K. At higher

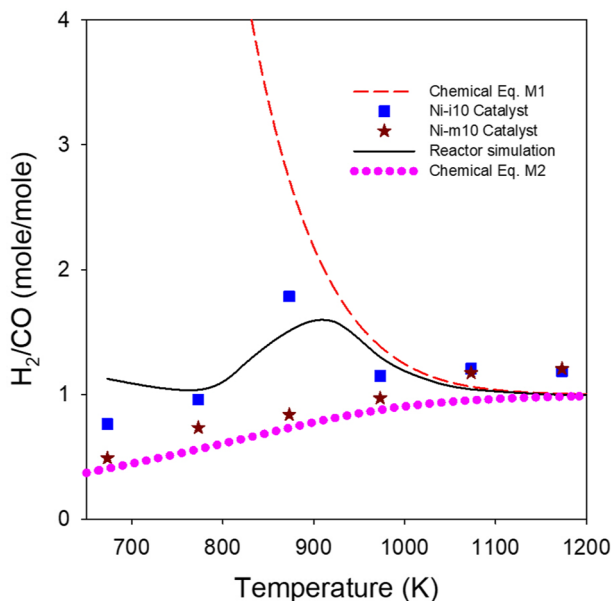


Fig. 4 H₂/CO ratio vs temperature. Experimental data (black star Ni-m10, black square Ni-i10), Chemical equilibrium calculations (M1 method: dashed line, M2 method: dotted), and reactor simulation (solid line) with an equimolar reaction mixture ($R = \text{CO}_2/\text{CH}_4 = 1$). The experimental data were obtained with $W/F_{\text{CH}_4} = 7.84 \times 10^{-6} \text{ g}_{\text{cat}} \text{ min cm}^{-3}$

temperatures, both the experimental and predicted ratios from the reactor simulation are close to the chemical equilibrium curves. As discussed above, the overprediction of reaction (Eq. 3) at low temperatures by the M1 method results in a higher amount of H₂, leading to higher H₂/CO ratios. In contrast, the M2 method predicts a gradual increase in this ratio as the temperature increases. It is observed that the simulations predict an H₂/CO ratio equal to unity at temperatures above 1073 K. However, as expected due to the lower CO amount obtained in the experiments, the H₂/CO ratio at high temperatures was slightly higher than that obtained in the simulations at the reactor outlet. As mentioned earlier, the Ni-m10 catalyst showed a slower reaction rate for the DRM compared with Ni-i10. This is clearly seen in Fig. 4, where the H₂/CO ratio for the Ni-m10 catalyst gradually increases with temperature, only approaching the reactor simulation curve at temperatures above 973 K. In the case of the Ni-i10 catalyst, the H₂/CO ratio followed the same trend as the reactor simulation curve from 773 K. The fact that the H₂/CO ratio obtained for Ni-i10 catalysts agrees most with the chemical equilibrium predicted using the M1 method at temperatures below 1000 K indicates that in this catalyst, reaction (Eq. 3) (CH₄ decomposition) is highly favored. This promotes higher H₂ production and, of course, a high amount of solid carbon on the catalyst, which leads to rapid deactivation. In contrast, the H₂/CO ratio for the Ni-m10 catalyst follows the same trend predicted by the M2 method, indicating that on this catalyst, reaction (Eq. 3) is less favored, resulting in slow carbon deposition on the catalyst. The decomposition of CH₄ on the catalyst surface has been proposed as the controlling step for the DRM process

[16, 25], thus the differences in the performance of the two catalysts are related with the form in which Ni active sites are found on the catalysts. For example, Arauconi et al. [26] conducted a thermodynamic study in which they found that Ni particles with a size greater than 10 nm promote the formation of solid carbon, and this promotion increases at higher pressure. They suggest that an optimal Ni particle size for minimizing carbon production is below 5 nm. On the other hand, it has been proposed that the DRM is a structure-sensitive reaction, where the activation of CH_4 and CO_2 depends on the shape and structure of the active sites [10]. Recently, Vogt et al. [27] conducted a study using a Ni/SiO₂ catalyst and found that the optimal size to suppress solid carbon formation is 2–3 nm. They also suggest that for larger particles (3 nm < particle size < 6 nm), the activation of oxidant compounds becomes the limiting step, which evidences the structure-sensitive character of DRM. This suggests that proposals for the reaction pathway, whether for chemical equilibrium or micro-kinetics models, should consider the state of the Ni sites to achieve greater precision in their predictions. However, this is not a trivial task to carry out, and it may not be easy to implement in practical conditions.

In order to validate whether the set of reactions (Eqs. 1–5) and the implemented calculations allow the reproduction of the behavior for the DRM reaction data reported by other authors, the prediction of the reactor simulation was compared with the experimental data reported by Barroso et al. [28]. They reported their data obtained by varying the spatial time and in conditions where the external mass transfer resistance was negligible. The comparison was done by normalizing the W/F ratio. For the data obtained from Barroso et al., this was achieved by using the highest spatial time of their experimental data, while for the reactor simulation, the spatial time before the curve of CO_2 conversion reached a pseudo-plateau was used (Fig. S3a and b). It was found that the reactor simulation curves for CH_4 conversion reasonably describe the behavior of the experimental data reported by Barroso et al. (Fig. S3c and d), mostly at high temperatures ($T \geq 848$ K). However, for the CO_2 conversion, they exhibit the opposite behavior, with the simulation only reasonably describing the experimental data at low temperatures ($T \leq 873$ K). It is difficult to identify the causes of the observed discrepancies between experimental and simulated data due to several experimental factors that affect the DRM reaction (active metal, metal loading, particle size of active metal, spatial time, temperature, etc.), and consequently the determination of the kinetic rate from such data. Nevertheless, these results support that the reactor simulation can be considered a good approximation to the DRM reaction and therefore can be useful for rationalizing the experimental data obtained with the synthesized catalysts.

On the other hand, the main drawback of the DRM process is the production of coke, which inhibits its industrial implementation. Therefore, it is important to identify the effects that can occur in the reactor in order to determine the best operating conditions and minimize the production of this undesirable byproduct, or ascertain if the catalyst formulation is effectively inhibiting the production of coke.

In Fig. 5, the production of solid carbon (coke) predicted by the chemical equilibrium using the M1 method is shown as a function of temperature for three representative reactor feeds ($R=0.8, 1, 1.2$). It can be observed that the production of coke is highly favored, mainly with an excess of CH_4 , but this decreases at high

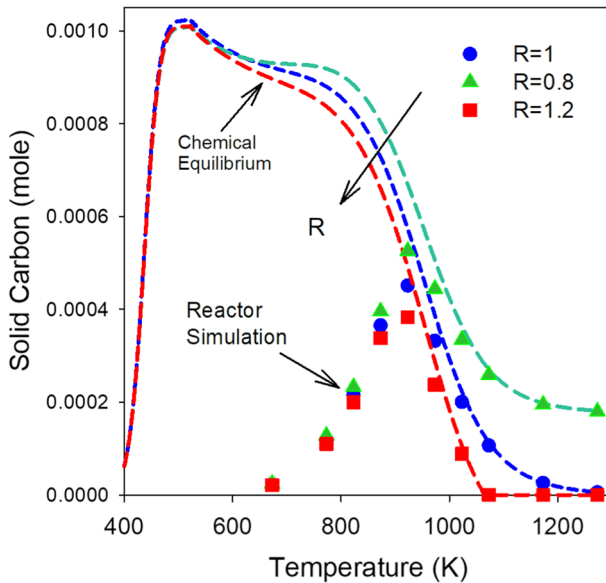


Fig. 5 Solid carbon (coke) production. Comparison between the chemical equilibrium prediction (M1 method) and reactor simulation at different temperatures. $R = \text{CO}_2/\text{CH}_4 = 0.8, 1.0, \text{ and } 1.2$

temperatures ($T > 950 \text{ K}$) and with high CO_2/CH_4 ratios, which is in agreement with other reports in the literature [1, 29, 30]. The calculations predict two peaks: as was discussed above, the first peak with the maximum at low temperature ($T \sim 550 \text{ K}$) is due to the overprediction of reaction (Eq. 3) by the M1 method; therefore, this peak could be discarded in the analysis for solid carbon production. From Fig. 1 (see CO_2 curve), it can be seen that the overprediction decreases around 800 K . Thus, the peak with the maximum around 900 K is related mainly to methane decomposition, because it can be observed that an excess of CH_4 in the reactor feed promotes this peak (Fig. 5). Although another possibility cannot be discarded, it has also been reported that the CO disproportionation reaction can contribute to solid carbon production in this temperature range [14]. Although coke production is thermodynamically favored, it does not necessarily mean that it is kinetically equally favored. From the reactor simulation, it was found that its production is kinetically significant above 700 K and reaches the chemical equilibrium curve between 900 and 1000 K . This finding is in good agreement with the experimental results reported by other authors (e.g., [31]). In the three selected cases, the reactor simulation aligns with the chemical equilibrium curve calculated using the M1 method for temperatures above 900 K . This alignment reinforcing that the set of reactions and the reactor simulation can reasonably describe the behavior of the DRM reaction. It is noteworthy from the reactor simulation that at temperatures below 800 K (Fig. 5), the production of coke could show only slight differences with the variation of the reactor feed ratio ($R = \text{CO}_2/\text{CH}_4$). The pressure of the reaction system was varied as an exercise to test the prediction capability of both reactor simulation and chemical equilibrium using the M1 method for solid carbon production. It was found that the M1 method

predicts a significant increase in solid carbon production as the pressure in the reactor increases (see Fig. S4a), while the reactor simulation predicts that there is an increase in solid carbon production, and its production shifts toward the reactor inlet (see Fig. S4b). These results are in good agreement with the reports of Nikko et al. [29] and the experimental results of Kahle et al. [25], supporting that the used reaction model and simulations are suitable for rationalizing the deactivation of the synthesized catalysts.

Based on the results in Fig. 5, it could be expected that under kinetically favorable conditions ($T > 900$ K), the production of coke decreases as the reactor temperature increases. Consequently, if a minor amount is produced, the catalyst should exhibit slow deactivation caused by the deposition of this byproduct. Typically, highly active

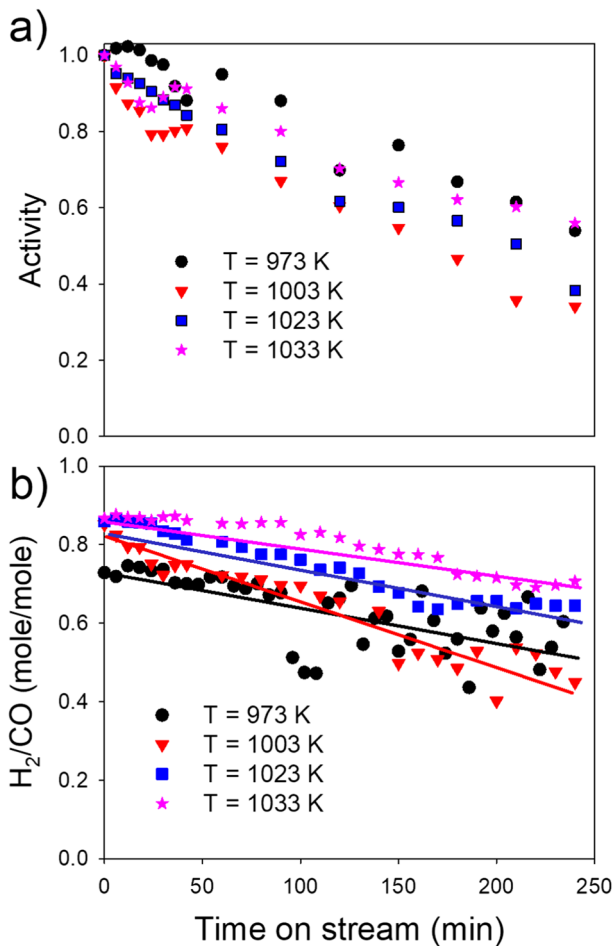


Fig. 6 Catalytic activity (a) and H₂/CO ratio (b) versus time on stream during the deactivation test for the Ni-m10 catalyst under the kinetic regime ($W/F_{\text{CH}_4} = 3.92 \times 10^{-7} \text{ g}_{\text{cat}} \text{ min cm}^{-3}$) at various reaction temperatures. $R = \text{CO}_2/\text{CH}_4 = 1$

catalysts also have a high rate of coke production [2] (as is the case with the Ni-i10 catalyst [22]). Therefore, it was decided to conduct deactivation experiments with the Ni-m10 catalyst at different temperatures to observe the changes in its deactivation. The reactor was operated under kinetic conditions ($W/F_{\text{CH}_4} = 3.92 \times 10^{-7} \text{ g}_{\text{cat}} \text{ min cm}^{-3}$) in order to prevent the masking effects due to external mass transport phenomena [22]. During the deactivation tests of the Ni-m10 catalyst, a different result from the prediction of the chemical equilibrium was observed (Fig. 6), as at lower temperatures, the catalyst showed a slower deactivation. The loss of catalytic activity ($a=r/r_0$) followed the temperature order, from highest to lowest: $1003 \text{ K} > 1023 \text{ K} > 1033 \text{ K} > 973 \text{ K}$. The temperature range used for the tests (973–1033 K) was chosen to minimize the possible sintering of Ni particles due to thermal effects. Additionally, the catalytic activity in the test at 1033 K was higher than at 1003 K, dismissing a significant effect of the Ni sintering on the results shown in Fig. 6. A previous study found that the main cause for the deactivation of the Ni-m10 catalyst was the encapsulation of Ni particles by coke [22].

The order of the deactivation curves depicted in Fig. 6 may be influenced by operational conditions within the reactor, which impact the chemical equilibrium of the reactions. It is well-known that reactor conditions can significantly affect catalyst deactivation [23]. Consequently, the reactor simulation was employed to investigate potential variations in the DRM reaction. This exploration involved varying the W/F_{CH_4} ratio (by adjusting the catalyst weight) while maintaining an equimolar reaction feed ($R=1$) and also varying the reaction temperature (as shown in Fig. 7). It was found from the simulation that for $W/F_{\text{CH}_4} \leq 6$, coke production is higher at lower temperatures and decreases when the reaction is performed at higher temperatures,

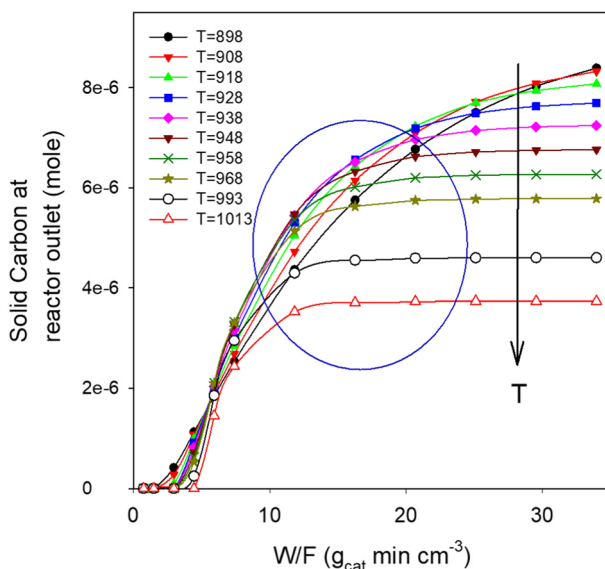


Fig. 7 Production of solid carbon (coke) versus W/F_{CH_4} ratio, obtained from the reactor simulation at various reaction temperatures. $R = \text{CO}_2/\text{CH}_4 = 1$

as expected from the chemical equilibrium (Fig. 5). However, under conditions where the spatial time is between 6 and 25, the production of coke could even be the reverse of what is expected from the chemical equilibrium for temperatures below 1013 K. For temperatures above 1013 K and with values of $W/F_{\text{CH}_4} \geq 25$, the trend of chemical equilibrium for the production of coke is recovered again, whereas the H_2/CO ratio calculated (Fig. S4b) follows the same complex behavior observed in Fig. 7. However, the difference in the magnitude of this ratio could be quite similar for values of $W/F_{\text{CH}_4} \leq 12$, suggesting that in practical conditions, it is necessary to operate the reactor at high spatial times ($W/F_{\text{CH}_4} > 20$) in order to observe substantial variations in the H_2/CO ratio. Fig. 6b shows the experimental H_2/CO ratio during the time on stream obtained with the Ni-m10 catalyst. It can be seen that the initial ratio at 1003 K, 1023 K, and 1033 K was practically the same (as expected due to the low spatial time in the reactor). However, the difference among the values of this ratio increased as the catalyst was deactivated. The solid lines in Fig. 6b were included only for better visualization of the activity loss because the experimental data became noisy (mainly at 973 K) due to the experimental difficulties in the measurement of H_2 production, given its low amount.

The experimental results presented in Fig. 6 can be explained through the simulation of the reactor depicted in Fig. 7. By analyzing the reaction rates at 908 K and 928 K, a potential reason for catalyst deactivation caused by coke formation was sought. These specific temperatures were chosen because, at the lower temperature, coke production is lower compared to the higher temperature, especially for values of W/F_{CH_4} around 12 (as shown in Fig. 7). Contrary to expectations, the catalyst exhibited slower deactivation at 908 K, which runs counter to the expected thermodynamic behavior. According to the simulation results, this effect is a consequence of the low spatial time in the reactor that prompts the shift of the chemical equilibrium, affecting mainly the reverse reactions shown in Eqs. 4 and 5. Among the calculated reaction rates, it was seen that at spatial times from 3 to 12 the disproportionation of CO is the most favored (Eq. 4) at 928 K (Fig. S5c). From a certain value of W/F_{CH_4} , each reaction approaches faster to the chemical equilibrium ($r=0$), with this approach being faster at higher temperatures (this is indicated in the Fig. S5c by the small vertical line where the curves for both temperatures intersect). Then, when the operating conditions in the reactor involve low spatial times and the temperature is below 1013 K (see Fig. 7), the DRM reaction can occur far from the chemical equilibrium conditions, favoring the production of the undesirable coke (solid carbon). A similar conclusion was expressed by Zambrano et al. [13], where they observed a maximum in the coke production as a function of the W/F_{CH_4} , concluding that the set of reactions shown in Eqs. 1–5 approaches the thermodynamic equilibrium in the reactor at high spatial times.

On the other hand, experimental deactivation tests were conducted to examine the effect of the CO_2/CH_4 ratio (R) on catalytic activity loss. Chemical equilibrium calculations reveal that operating with $R > 1$ reduces coke production (as shown in Fig. 5). Additionally, if the reactor operates at low spatial times, the disproportionation of CO could be highly favored (as indicated in Fig. S5c). Considering these effects, the reactor was operated under kinetic conditions ($W/F_{\text{CH}_4} = 3.92 \times 10^{-7} \text{ g min cm}^{-3}$) at a temperature of 1073 K, because the reactor

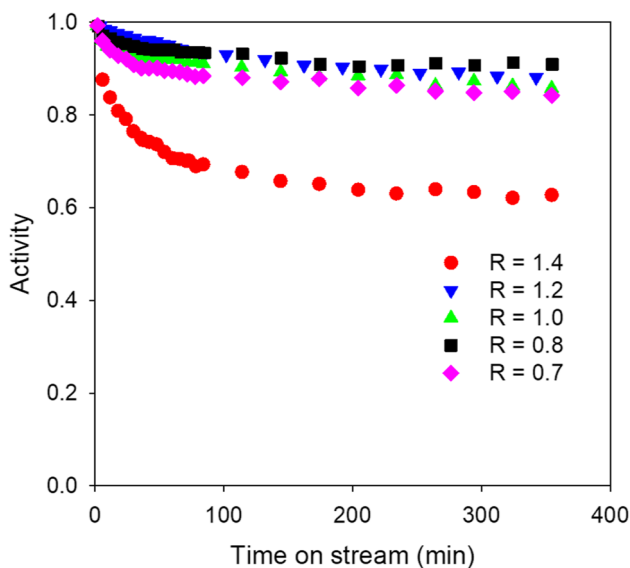


Fig. 8 Catalytic activity versus time on stream for the Ni-m10 catalyst at 1073 K at various CO_2/CH_4 (R) ratios. The experimental data were obtained in kinetic conditions ($W/F_{\text{CH}_4} = 3.92 \times 10^{-7} \text{ g}_{\text{cat}} \text{ min cm}^{-3}$)

simulation showed that above 1013 K the coke production curves for different temperatures do not intersect (see Fig. 7). In Fig. 8, the resultant deactivation curves are shown, revealing that the catalyst lost its activity faster with $R = 1.4$ compared to when lower values of this ratio were used ($0.8 < R < 1.2$). These results suggest that when the reactor operates far from chemical equilibrium, the disproportionation of CO significantly affects the deactivation of the Ni catalyst by promoting coke production. Calgaro et al. [30] reported that the coke deposition on a Ni–Mg–Al catalyst could be controlled by using $R = 2$, which contrasts with our experimental findings. In our experiments, the Ni-m10 catalyst rapidly deactivated due to coke formation with $R = 1.4$. The discrepancies between the two studies can be attributed not only to the different catalytic activity of the studied solids based on their composition but also to variations in the operating conditions within the reactor. In their experiments with different spatial times, they observed that coke production did not exhibit a proportional relationship with the W/F_{CH_4} ratio (1.2, 2.5, 4.5, and 9.3 g h/mol). In fact, with both the lowest and highest spatial time, the production of coke was lower than that produced with the reactor operating at the intermediate W/F_{CH_4} ratios. Their results can be rationalized with the results of the reactor simulation shown in Fig. 7.

Based on the reactor simulation findings, it can be observed that both the reverse of reaction (Eq. 2) and the reverse of reaction (Eq. 4) are favored under high spatial time conditions ($4 < W/F_{\text{CH}_4} < 15$). Both reverse reactions follow the same trend (see Fig. S5c). This indicates that spatial time has an important effect on CO_2 activation at catalytic sites, resulting in the inhibition of CO_2 adsorption due to the low residence time of the reaction mixture in the catalytic bed. Consequently, the deficiency

of adsorbed oxygen atoms prevents the formation of intermediate species such as O(s) and OH(s) [16, 17, 25], leading to rapid solid carbon formation on the active sites. This suggests that spatial time can promote a kinetic effect comparable to that observed for large Ni particles in solid carbon formation [27].

The chemical equilibrium in a chemical reactor can be shifted by manipulating the operating conditions to favor the formation of desired compounds. However, in the case of the DRM reaction performed with Ni-based catalysts, this advantage does not seem to apply. The experimental results and reactor simulations indicate that operating the reactor far from chemical equilibrium could promote coke production through the disproportionation of CO. Finally, it can be deduced from the experimental and simulation results that the effect of reactor operation conditions on coke production will strongly depend on the intrinsic activity of the catalyst. This dependence arises because the W/F_{CH_4} ratio is directly related to the amount of catalyst loaded in the reactor, especially for solids with high catalytic activity. Similarly, the CO_2/CH_4 ratio (R) has a significant effect, but its impact is also influenced by the reactor's operating conditions. Consequently, the catalytic study of solids being evaluated for the DRM reaction should consider the operational conditions of the reactor, determining whether the reactor operates close to chemical equilibrium or not. This allows for conclusive assessment of the obtained reaction information (e.g., selectivity, resistance against deactivation, etc.), which instills confidence in interpreting data without bias arising from the operational conditions. Furthermore, as observed from the chemical equilibrium calculations using the M1 and M2 methods and in the literature reports [16, 17, 25], finding a model that completely aligns with the experimental results remains challenging due to several factors influencing the reaction. In this context, studies involving proposals with elementary steps (whether for chemical equilibrium or micro-kinetics modeling) gain relevance. However, it is crucial to ensure that the reactor operates under conditions where the obtained data satisfy theoretical assumptions (for example, achieving chemical equilibrium at the reactor outlet).

Conclusions

The dry reforming of methane (DRM) was investigated by conducting chemical equilibrium calculations and simulating the reactor using a pseudo-homogeneous model. These calculations were then contrasted with experimental results obtained using Ni-based catalysts in a reactor operating under both low and high spatial time conditions. Both sets of calculations reasonably describe the experimental results obtained at high spatial time (close to chemical equilibrium). However, deactivation tests performed under kinetic conditions (low spatial time) revealed that the Ni-m10 tested catalyst lost its catalytic activity more rapidly at 928 K compared to 908 K, which contradicts the prediction based on chemical equilibrium. From the reactor simulation, a range of spatial time (W/F_{CH_4}) was observed where the proposed reactions significantly deviate from chemical equilibrium. This deviation results in both the water gas shift reaction and the disproportionation of CO, leading to rapid catalyst deactivation due to solid carbon deposition. Even under conditions where the

reactor feed contains an excess of CO₂ (CO₂/CH₄ > 1), this effect persists. The cause of this rapid deactivation can be attributed to the kinetic inhibition of CO₂ adsorption at high spatial time, which hinders the activation of this molecule on the catalytic sites. Consequently, the surface species such as O(s) and OH(s) do not form in sufficient quantities, which contributes to the rapid formation of solid carbon. Ultimately, in practical terms, the consideration of low or high spatial time in the reactor will depend on the intrinsic catalytic activity of the solid. Therefore, this aspect should be carefully taken into account to avoid biasing the information obtained from the experimental data.

Supplementary Information The online version contains supplementary material available at <https://doi.org/10.1007/s11144-024-02658-2>.

Acknowledgements The author gratefully acknowledges the contribution of Eric Flores-Elizondo and Victor G. de la Cruz-Flores, who obtained part of the experimental results during their studies to obtain a master's degree.

Funding This work was supported by grants from CONACYT (Project No. 156064) and UANL (PAICYT No. IT550-10).

Declarations

Competing interests The author has no competing interests to declare that are relevant to the content of this article.

Content of the publication During the preparation of this work, the author used ARIA and Copilot (Opera and Microsoft Edge Browsers) in order to improve language and readability, and the author reviewed and edited the content as needed and takes full responsibility for the content of the publication.

References

1. Sandoval-Diaz LE, Schlögl R, Lunkenbein T (2022) Quo Vadis dry reforming of methane? A review on its chemical, environmental, and industrial prospects. *Catalysts* 12:465. <https://doi.org/10.3390/catal12050465>
2. Wittich K, Krämer M, Bottke N, Schunk SA (2020) Catalytic dry reforming of methane: insights from model systems. *ChemCatChem* 12:2130–2147. <https://doi.org/10.1002/cctc.201902142>
3. Li M, Sun Z, Hu YH (2022) Thermo-photo coupled catalytic CO₂ reforming of methane: a review. *Chem Eng J* 428:131222. <https://doi.org/10.1016/j.cej.2021.131222>
4. Vakili R, Gholami R, Stere CE et al (2020) Plasma-assisted catalytic dry reforming of methane (DRM) over metal-organic frameworks (MOFs)-based catalysts. *Appl Catal B Environ* 260:118195. <https://doi.org/10.1016/j.apcatb.2019.118195>
5. Li M, Sun Z, Hu YH (2021) Catalysts for CO₂ reforming of CH₄: a review. *J Mater Chem A* 9:12495–12520. <https://doi.org/10.1039/D1TA00440A>
6. Alenazey FSh (2014) Utilizing carbon dioxide as a regenerative agent in methane dry reforming to improve hydrogen production and catalyst activity and longevity. *Int J Hydrog Energy* 39:18632–18641. <https://doi.org/10.1016/j.ijhydene.2014.02.148>
7. Owgi AHK, Jalil AA, Hussain I et al (2021) Catalytic systems for enhanced carbon dioxide reforming of methane: a review. *Environ Chem Lett* 19:2157–2183. <https://doi.org/10.1007/s10311-020-01164-w>
8. Lavoie JM (2014) Review on dry reforming of methane, a potentially more environmentally-friendly approach to the increasing natural gas exploitation. *Front Chem* 2:81. <https://doi.org/10.3389/fchem.2014.00081>

9. Iyer MV, Norcio LP, Kugler EL, Dadyburjor DB (2003) Kinetic modeling for methane reforming with carbon dioxide over a mixed-metal carbide catalyst. *Ind Eng Chem Res* 42:2712–2721. <https://doi.org/10.1021/ie020677q>
10. Bradford MCJ, Vannice MA (1999) CO₂ reforming of CH₄. *Catal Rev* 41:1–42. <https://doi.org/10.1081/CR-100101948>
11. Bartholomew CH (2001) Mechanisms of catalyst deactivation. *Appl Catal Gen* 212:17–60. [https://doi.org/10.1016/S0926-860X\(00\)00843-7](https://doi.org/10.1016/S0926-860X(00)00843-7)
12. Rostrup-Nielsen JR (1997) Industrial relevance of coking. *Catal Today* 37:225–232. [https://doi.org/10.1016/S0920-5861\(97\)00016-3](https://doi.org/10.1016/S0920-5861(97)00016-3)
13. Zambrano D, Soler J, Herguido J, Menéndez M (2019) Kinetic study of dry reforming of methane over Ni–Ce/Al₂O₃ catalyst with deactivation. *Top Catal* 62:456–466. <https://doi.org/10.1007/s11244-019-01157-2>
14. Ginsburg JM, Piña J, El Solh T, de Lasa HI (2005) Coke formation over a nickel catalyst under methane dry reforming conditions: thermodynamic and kinetic models. *Ind Eng Chem Res* 44:4846–4854. <https://doi.org/10.1021/ie0496333>
15. Benguerba Y, Dehimi L, Virginie M et al (2015) Modelling of methane dry reforming over Ni/Al₂O₃ catalyst in a fixed-bed catalytic reactor. *React Kinet Mech Catal* 114:109–119. <https://doi.org/10.1007/s11444-014-0772-5>
16. Delgado KH, Maier L, Tischer S et al (2015) Surface reaction kinetics of steam- and CO₂-reforming as well as oxidation of methane over nickel-based catalysts. *Catalysts* 5:871–904. <https://doi.org/10.3390/catal5020871>
17. Rakhi GV, Mauss F (2023) Insights into dry reforming of methane over nickel catalyst using a thermodynamic model. *React Kinet Mech Catal* 136:1197–1210. <https://doi.org/10.1007/s11444-023-02426-8>
18. Scilab, version 6.1.0. <https://www.scilab.org>. Accessed 28 Apr 2024
19. DWSIM—The Open Source Chemical Process Simulator (2024) Chemical process simulation for everyone: DWSIM for desktop is free and open-source. <https://dwsim.org/>. Accessed 28 Apr 2024
20. Cherbański R, Franczyk E, Lewak M et al (2021) Modelling of methane dry reforming over Ni/CaO–Al₂O₃ catalyst. *Chem Process Eng* 42(3):235–252
21. Raybaut P (2009) Spyder-documentation. <https://www.spyder-ide.org/>. Accessed 28 Apr 2024
22. de la Cruz-Flores VG, Martinez-Hernandez A, Gracia-Pinilla MA (2020) Deactivation of Ni-SiO₂ catalysts that are synthesized via a modified direct synthesis method during the dry reforming of methane. *Appl Catal Gen* 594:117455. <https://doi.org/10.1016/j.apcata.2020.117455>
23. Moulijn JA, van Diepen AE, Kapteijn F (2001) Catalyst deactivation?: what to do? *Appl Catal Gen* 212:3–16. [https://doi.org/10.1016/S0926-860X\(00\)00842-5](https://doi.org/10.1016/S0926-860X(00)00842-5)
24. Froment GF (2001) Modeling of catalyst deactivation. *Appl Catal Gen* 212:117–128. [https://doi.org/10.1016/S0926-860X\(00\)00850-4](https://doi.org/10.1016/S0926-860X(00)00850-4)
25. Kahle LCS, Roussière T, Maier L et al (2013) Methane dry reforming at high temperature and elevated pressure: impact of gas-phase reactions. *Ind Eng Chem Res* 52:11920–11930. <https://doi.org/10.1021/ie401048w>
26. Abdel Karim Aramouni N, Zeaiter J, Kwapinski W, Ahmad MN (2017) Thermodynamic analysis of methane dry reforming: effect of the catalyst particle size on carbon formation. *Energy Convers Manag* 150:614–622. <https://doi.org/10.1016/j.enconman.2017.08.056>
27. Vogt C, Kranenborg J, Monai M, Weckhuysen BM (2020) Structure sensitivity in steam and dry methane reforming over nickel: activity and carbon formation. *ACS Catal* 10:1428–1438. <https://doi.org/10.1021/acscatal.9b04193>
28. Barroso Quiroga MM, Castro Luna AE (2007) Kinetic analysis of rate data for dry reforming of methane. *Ind Eng Chem Res* 46:5265–5270. <https://doi.org/10.1021/ie061645w>
29. Nikoo MK, Amin NAS (2011) Thermodynamic analysis of carbon dioxide reforming of methane in view of solid carbon formation. *Fuel Process Technol* 92:678–691. <https://doi.org/10.1016/j.fuproc.2010.11.027>
30. Calgaro CO, Rocha AL, Perez-Lopez OW (2020) Deactivation control in CO₂ reforming of methane over Ni–Mg–Al catalyst. *React Kinet Mech Catal* 130:159–178. <https://doi.org/10.1007/s11444-020-01770-3>
31. Al-Otaibi F, Xiao H, Berrouk AS, Polychronopoulou K (2023) Numerical study of dry reforming of methane in packed and fluidized beds: effects of key operating parameters. *ChemEng* 7:57. <https://doi.org/10.3390/chemengineering7030057>

Publisher's Note Springer Nature remains neutral with regard to jurisdictional claims in published maps and institutional affiliations.

Springer Nature or its licensor (e.g. a society or other partner) holds exclusive rights to this article under a publishing agreement with the author(s) or other rightsholder(s); author self-archiving of the accepted manuscript version of this article is solely governed by the terms of such publishing agreement and applicable law.